SOURCE DATA · TRANSPARENT PROCESS · OPEN ACCESS

EMBO *reports*

Developmental cell death of cortical projection neurons is controlled by a Bcl11a/Bcl6-dependent pathway

Christoph Wiegreffe[1], Tobias Wahl[1], Natalie Sophie Joos[1,†], Jerome Bonnefont[2,3] ID, Pentao Liu[4] & Stefan Britsch[1,*] ID

Abstract

Developmental neuron death plays a pivotal role in refining organization and wiring during neocortex formation. Aberrant regulation of this process results in neurodevelopmental disorders including impaired learning and memory. Underlying molecular pathways are incompletely determined. Loss of Bcl11a in cortical projection neurons induces pronounced cell death in upper-layer cortical projection neurons during postnatal corticogenesis. We use this genetic model to explore genetic mechanisms by which developmental neuron death is controlled. Unexpectedly, we find Bcl6, previously shown to be involved in the transition of cortical neurons from progenitor to postmitotic differentiation state to provide a major checkpoint regulating neuron survival during late cortical development. We show that Bcl11a is a direct transcriptional regulator of *Bcl6*. Deletion of *Bcl6* exerts death of cortical projection neurons. In turn, reintroduction of *Bcl6* into *Bcl11a* mutants prevents induction of cell death in these neurons. Together, our data identify a novel Bcl11a/Bcl6-dependent molecular pathway in regulation of developmental cell death during corticogenesis.

Introduction

Developmental cell death (DCD) occurs in all animals and organs. It is part of a homeostatic balance between generation and elimination of cells. Developmental cell death provides a major checkpoint for quality control allowing selective removal of either defective, mis-integrated or no longer required cells (Causeret *et al*, 2018; Wong & Marin, 2019). During the development of the mammalian neocortex, excess numbers of neurons are generated. Supernumerary neurons are eliminated during two distinct waves of apoptosis. In mice, the first wave of DCD occurs around E14 and affects predominantly proliferating neuron precursors (Blaschke *et al*, 1996; de la Rosa & de Pablo, 2000; Roth *et al*, 2000). During a second wave, corresponding to the first two postnatal weeks in rodents, approximately 30% of postmitotic cortical neurons are eliminated by DCD (Verney *et al*, 2000; Southwell *et al*, 2012). Within this period, entire neuron populations, as for example Cajal–Retzius cells, which transiently serve as signaling centers, are removed by DCD (Chowdhury *et al*, 2010; Ledonne *et al*, 2016), while in other neuron types, like cortical projection neurons (CPN), DCD adjusts definitive neuron numbers and refines immature synaptic circuits (Blanquie *et al*, 2017; Wong *et al*, 2018). In the neocortex, dysregulated DCD has been shown to be associated with a wide spectrum of neurodevelopmental disorders, including major structural changes as well as structurally more subtle defects, like autism-spectrum disorders and intellectual disability (Kuida *et al*, 1996; Eriksson *et al*, 2001; Wei *et al*, 2014; Nakamura *et al*, 2016). Developmental cell death acts cell-type specific and is spatio-temporarily highly restricted suggesting complex molecular regulation. In contrast to the peripheral nervous system, where target-derived neurotrophic signals have been extensively demonstrated to play a key role in regulation of neuron survival (Huang & Reichardt, 2001), the molecular controls of DCD within the central nervous system (CNS) are incompletely determined. Electrical and synaptic activity has been shown to confer survival signals onto postmitotic cortical neurons (Blanquie *et al*, 2017; Denaxa *et al*, 2018; Priya *et al*, 2018; Wong *et al*, 2018). Transcription factor cascades as well as secreted signaling molecules are of key importance for the development of the neocortex. It is, however, unclear, how these regulatory networks are connected to DCD.

1   Institute of Molecular and Cellular Anatomy, Ulm University, Ulm, Germany
2   Institut de Recherche Interdisciplinaire en Biologie Humaine et Moléculaire (IRIBHM), and ULB Neuroscience Institute (UNI), Université Libre de Bruxelles (ULB), Brussels, Belgium
3   VIB-KU Leuven Center for Brain & Disease Research, KU Leuven Department of Neuroscience, Leuven Brain Institute, Leuven, Belgium
4   School of Biomedical Sciences, Li Ka Shing Faculty of Medicine, The University of Hong Kong, Hong Kong, China
    *Corresponding author. Tel: +49 (0) 731 500 23101; Fax: +49 (0) 731 500 23102, E-mail: stefan.britsch@uni-ulm.de
    †Present address: Department of Internal Medicine I, University Hospital Ulm, Ulm, Germany

Bcl11a (*Ctip1*) encodes a zinc-finger protein that regulates transcription through interaction with COUP-TF proteins as well as direct, sequence-dependent DNA binding (Avram *et al*, 2002). We previously demonstrated that postmitotic upper-layer CPN require expression of Bcl11a for early postnatal survival. Cre/loxP-dependent ablation of *Bcl11a* in CPN results in massive increase in apoptosis between P4 and P6 selectively in upper-layer CPN (Wiegreffe *et al*, 2015).

In this study, we employed *Bcl11a* mutation in CPN as a highly selective genetic tool to systematically identify downstream candidate genes involved in the regulation of DCD in postmitotic CPN. Using comparative transcriptome analysis, we found that Bcl6, previously reported to be involved in the transition of cortical neurons from progenitor to postmitotic differentiation state (Tiberi *et al*, 2012; Bonnefont *et al*, 2019), is downregulated in *Bcl11a* mutant upper-layer CPN. Furthermore, we show Bcl11a to directly bind to a conserved promotor element and to activate transcription of the *Bcl6* gene. Knockout of *Bcl6* in postmitotic CPN induces their apoptosis. In turn, reintroduction of *Bcl6* into *Bcl11a* mutant CPN prevents these neurons from apoptosis. Finally, we show *Foxo1* to be downregulated in both, *Bcl6* and *Bcl11a* mutant CPN. Normalization of *Foxo1* expression is sufficient to suppress increased apoptosis in *Bcl11a* mutant CPN suggesting Foxo1 to participate in the regulation of DCD in CPN during postnatal neocorticogenesis. Taken together, in this study we demonstrate that DCD of postmitotic upper-layer CPN is controlled by a novel Bcl11a/Bcl6-dependent transcriptional pathway.

Results and Discussion

Identification of downstream candidate targets of Bcl11a

We used *Bcl11a*$^{F/F}$*; Emx1*^{IRESCre} brains as a model to identify genes that play a role in postnatal survival of projection neurons in the somatosensory neocortex. *Bcl11a* mutant brains display robust increase in apoptosis during the second wave of DCD in upper cortical layers at postnatal stages (Wiegreffe *et al*, 2015). Using laser capture microdissection, we specifically isolated cortical layers 2–4 of *Bcl11a* mutant and control brains at P2 (Fig 1A and B), a stage
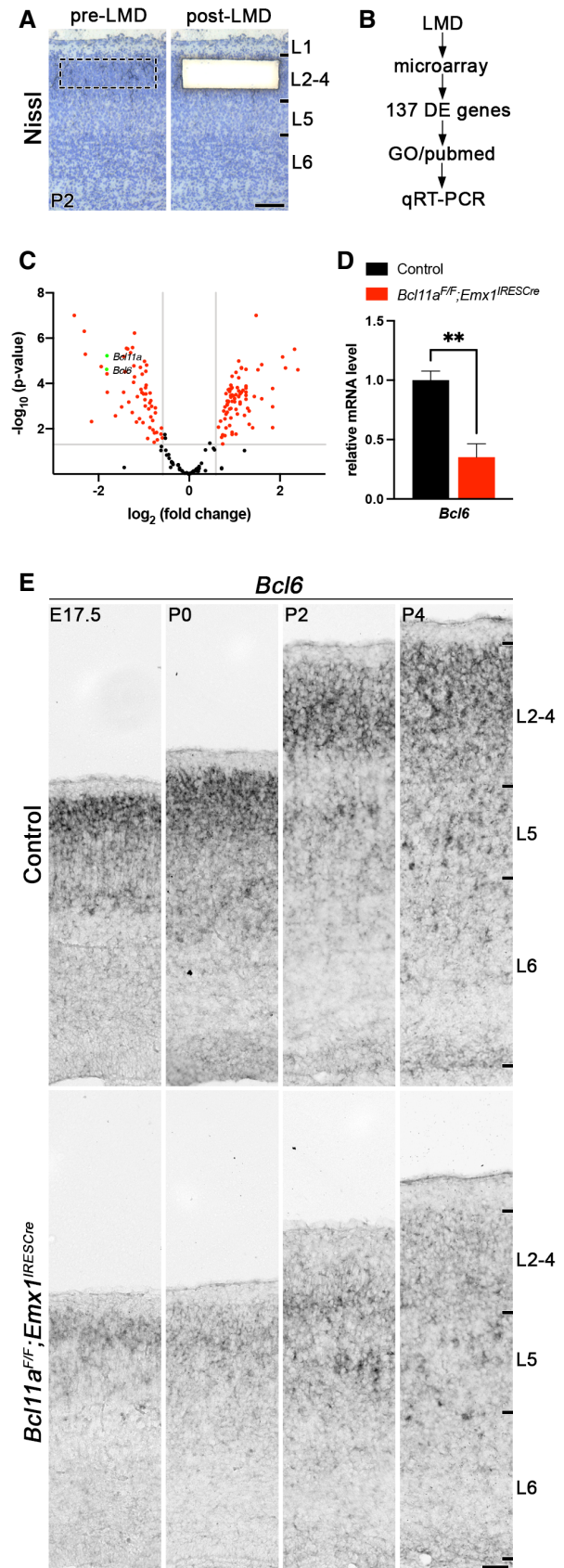
Figure 1.   Identification of downstream candidate target genes of Bcl11a in superficial cortical layers at early postnatal development.

A   Cortical layers 2–4 were isolated by laser microdissection from *Bcl11a*$^{F/F}$*; Emx1*^{IRESCre} and control neocortex (*n* = 4).

B   Gene expression was compared using microarrays. From a set of 137 differentially expressed (DE) genes, candidate targets were selected based on gene ontology (GO) and PubMed analyses and verified by quantitative real-time PCR and RNA *in situ* hybridization.

C   Volcano plot showing DE genes (red). Those not significantly changed (fold change < 1.5; *P* > 0.05) are shaded black. Bcl11a and Bcl6 are highlighted in green.

D   Relative *Bcl6* mRNA expression level determined by quantitative real-time PCR is decreased in laser-microdissected cortical tissue of P2 *Bcl11a*$^{F/F}$*; Emx1*^{IRESCre} compared with control brains (*n* = 4). Results are expressed as mean ± s.e.m.; Student's *t*-test; **P < 0.01.

E   RNA *in situ* hybridization showing downregulation of *Bcl6* expression in *Bcl11a*$^{F/F}$*;Emx1*^{IRESCre} compared with control neocortex at E17.5, P0, P2, and P4.

Data information: Scale bars, 100 μm (A) and 50 μm (E).

when the second wave of apoptosis has not yet been initiated (Blanquie *et al*, 2017) and cell death is not yet increased in *Bcl11a* mutants (Wiegreffe *et al*, 2015). We then performed a differential expression analysis using microarrays and identified a set of 137 differentially expressed (DE) genes that were subjected to a GO overrepresentation test as previously described (Mi *et al*, 2013; De Bruyckere *et al*, 2018), which revealed genes involved in axon guidance, cell–cell adhesion, and regulation of cell communication (Figs 1C, and EV1, EV2 and EV3A; Dataset EV1). To verify the validity of the experimental approach, selected candidate genes were tested by quantitative real-time PCR and RNA *in situ* hybridization. *Cdh6*, *Cdh12*, *Efna5*, and *Pcdh9* that were identified as downregulated were verified by this approach (Fig EV3B and C). In addition, *Cdh13*, *Flrt2*, *Flrt3*, and *Slit2* were verified as upregulated (Fig EV3B and D). Together, these results show that our genetic approach consistently identified DE genes in upper cortical layers of *Bcl11a* mutant brains that could directly or indirectly be involved in the regulation of developmental apoptosis.

Among the DE genes, we found *Bcl6*, a transcriptional repressor that was previously reported to regulate cortical neurogenesis (Tiberi *et al*, 2012; Bonnefont *et al*, 2019), to be downregulated by $64.8 \pm 0.1\%$ in *Bcl11a* mutant neocortex (Fig 1D). Using RNA *in situ* hybridization, we found robust expression of *Bcl6* predominantly in upper and at low levels in deep cortical layers of controls between E17.5 and P4 (Fig 1E). In *Bcl11a* mutant neocortex, *Bcl6* was downregulated in upper cortical layers at these stages (Fig 1E), suggesting this gene to be transcriptionally downstream of Bcl11a in upper cortical layers. Outside the CNS, Bcl6 exerts anti-apoptotic functions by suppressing genes involved in DNA damage response (Phan & Dalla-Favera, 2004; Phan *et al*, 2005; Ranuncolo *et al*, 2007), which could possibly be conserved in the developing neocortex as well. Therefore, we focused further analyses on Bcl6.

Bcl6 is a direct target of Bcl11a in upper-layer cortical projection neurons

To better characterize the expression of Bcl6 protein in early postnatal somatosensory cortex we generated a polyclonal antibody in guinea pig raised against the N-terminal 484 amino acids of mouse Bcl6. Specificity of the Bcl6 antibody was tested by immunohistochemistry using *Bcl6* mutant brains, which lack exons 4–10 (Ye

et al, 1997) and do not express Bcl6 protein (Tiberi *et al*, 2012). In comparison to wild-type littermates, we did not detect Bcl6 protein in *Bcl6* mutant brains at P0 (Appendix Fig S1), demonstrating our antibody to specifically detect Bcl6 protein. Coexpression analysis of Bcl6 together with Bcl11a and Satb2, a marker for callosal projection neurons (Alcamo *et al*, 2008; Britanova *et al*, 2008), showed $25.6 \pm 1.9\%$ Bcl6$^+$ Bcl11a$^+$ Satb2$^+$, $1.3 \pm 0.5\%$ Bcl6$^+$ Bcl11a$^+$, and $0.8 \pm 0.2\%$ Bcl6$^+$ Satb2$^+$ cells in wild-type brains. Only $0.3 \pm 1.0\%$ of cells exclusively expressed Bcl6 (Fig 2A and B). Coexpression analysis of Bcl6 together with Bcl11a and Cux1, a marker for cortical layers 2–4 (Nieto *et al*, 2004), showed $19.0 \pm 0.7\%$ Bcl6$^+$ Bcl11a$^+$ Cux1$^+$, $11.6 \pm 0.9\%$ Bcl6$^+$ Bcl11a$^+$, and $1.0 \pm 0.2\%$ Bcl6$^+$ Cux1$^+$ cells. Again, only $0.9 \pm 0.2\%$ of cells exclusively expressed Bcl6 (Fig 2C and D). Thus, more than 90% of Bcl6$^+$ cells coexpress Satb2 as well as Bcl11a and more than 61% of these cells are located in Cux1$^+$ upper layers with distinct localization to cortical layers 2/3 (Fig 2C). Notably, a substantial proportion of Bcl6$^+$ cells is located in deep cortical layers. Thus, Bcl6 is a marker for a subset of callosal projection neurons identified by coexpression of Bcl11a and that are located in cortical layers 2/3 as well as in deep cortical layers.

By DNA sequence analysis, we found a TGACCA binding motif of Bcl11a (Liu *et al*, 2018) in the first intron that was located 982 bp downstream of the transcriptional start site and ~10.2 kb upstream of the first protein-coding exon of the *Bcl6* gene. This binding motif was embedded within a 55 bp long conserved region with a high degree of conservation between rat, human, and chimp (Fig 2E). Binding of Bcl11a to this motif was tested by chromatin immunoprecipitation (ChIP) followed by quantitative real-time PCR using a primer pair flanking this region. An enrichment of more than fourfold was found using a Bcl11a-specific antibody in comparison with an immunoglobulin G (IgG) control antibody (Fig 2F), demonstrating binding of Bcl11a to this region. As negative controls, binding of Bcl11a to exon 5 of *Bcl6* and the *Hprt* promoter was tested, but no significant enrichment was found in comparison with the IgG control antibody (Fig 2F). The sequence containing the Bcl11a binding motif was further tested for its ability to activate gene expression. In luciferase assays, a 1.5-fold induction was measured, indicating this element to convey functional activation upon Bcl11a binding (Fig 2G). As negative controls, we tested a region of exon 5 of the *Bcl6* gene as well as activation in the presence of the closely

---

Figure 2. Bcl6 is expressed in superficial callosal projection neurons and a target gene of Bcl11a.

A Immunohistochemistry of Bcl6 (red), Bcl11a (green), and Satb2 (blue) in P2 wild-type neocortex.

B Venn diagram displaying the proportions of Bcl6 neurons overlapping with Bcl11a and Satb2 expressing cells. The percentage of each labeled cell population is given in relation to all labeled cells (Bcl6$^+$ and Bcl11a$^+$ and Satb2$^+$, in total 4,479 cells).

C Immunohistochemistry of Bcl6 (red), Bcl11a (green), and Cux1 (blue) in P2 wild-type neocortex.

D Venn diagram displaying the proportions of Bcl6 neurons overlapping with Bcl11a and Cux1 expressing cells. The percentage of each labeled cell population is given in relation to all labeled cells (Bcl6$^+$ and Bcl11a$^+$ and Cux1$^+$, in total 4,301 cells).

E Scheme of the *Bcl6* gene locus displaying the start codon (ATG) at +11.2 kb relative to the transcriptional start site (TSS). A regulatory element (RE) in the first intron at +982 bp contains a conserved binding motif (TGACCA, in red) of Bcl11a.

F ChIP analysis using a Bcl11a antibody and P2 cortical tissue detects Bcl11a binding to the RE shown in (E). Negative controls include ChIP with unspecific IgG antibody and the precipitation of exon 5 of *Bcl6* and the *Hprt* promoter. The experiment was independently repeated four times. Results are expressed as mean ± s.e.m.; Student's *t*-test; *$P < 0.05$.

G Luciferase assays in HEK293 cells transfected with control (CAG-Ctl^{GFP}), Bcl11a (CAG-$Bcl11a^{GFP}$), or Bcl11b (CAG-$Bcl11b^{GFP}$) expression vector show induction of luciferase activity of the RE reporter construct by Bcl11a. Negative controls include a reporter construct for a region of exon 5 of the *Bcl6* gene and co-transfection with the closely related transcription factor Bcl11b. The experiment was independently repeated four times. Results are expressed as mean ± s.e.m.; one-way ANOVA followed by Tukey's *post-hoc* test; ***$P < 0.001$. Data information: Scale bars, 50 μm.
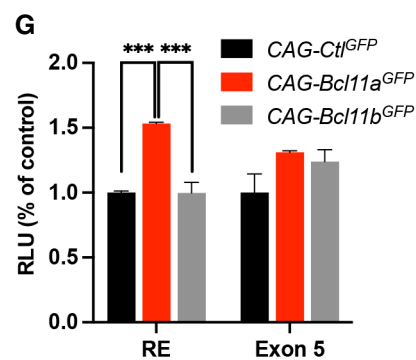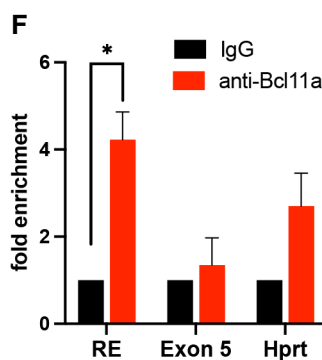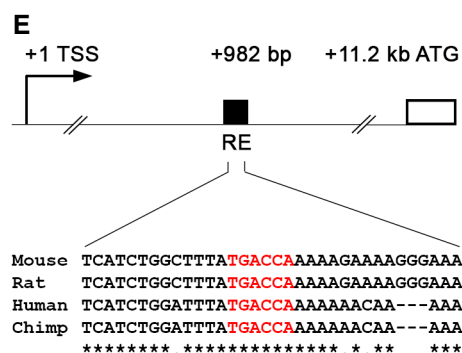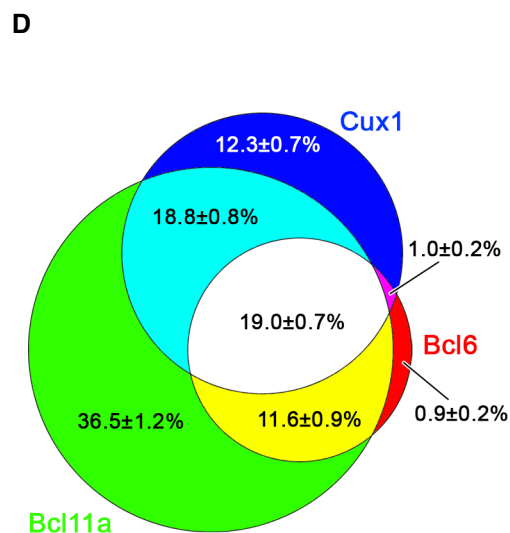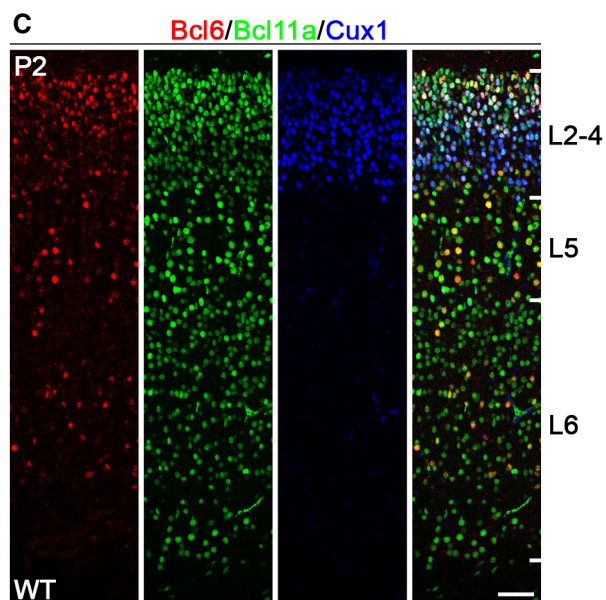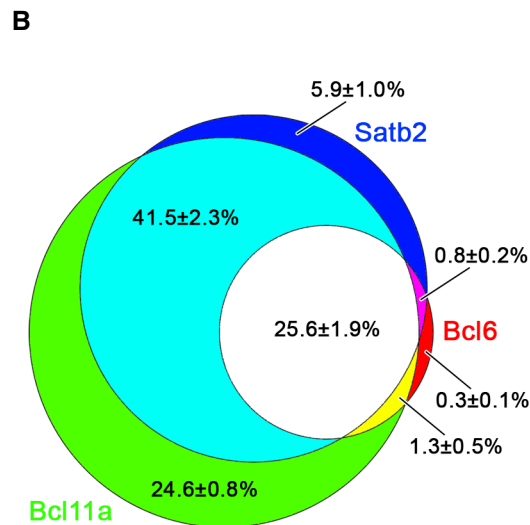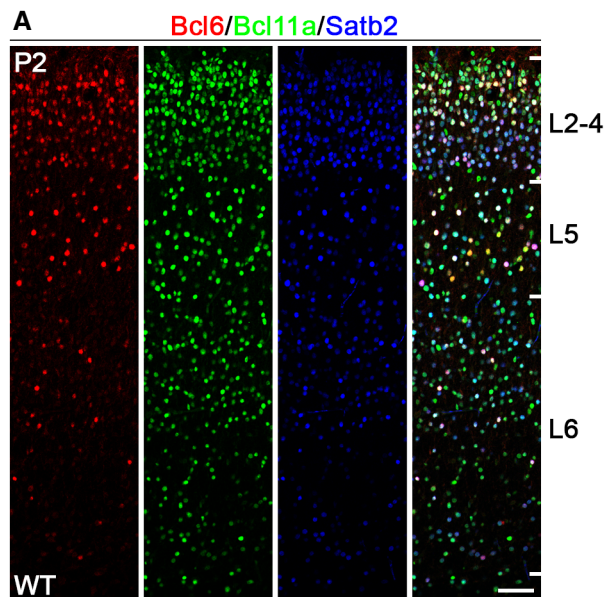
Figure 2.

related transcription factor Bcl11b, which both did not induce transcriptional activity in luciferase assays (Fig 2G).

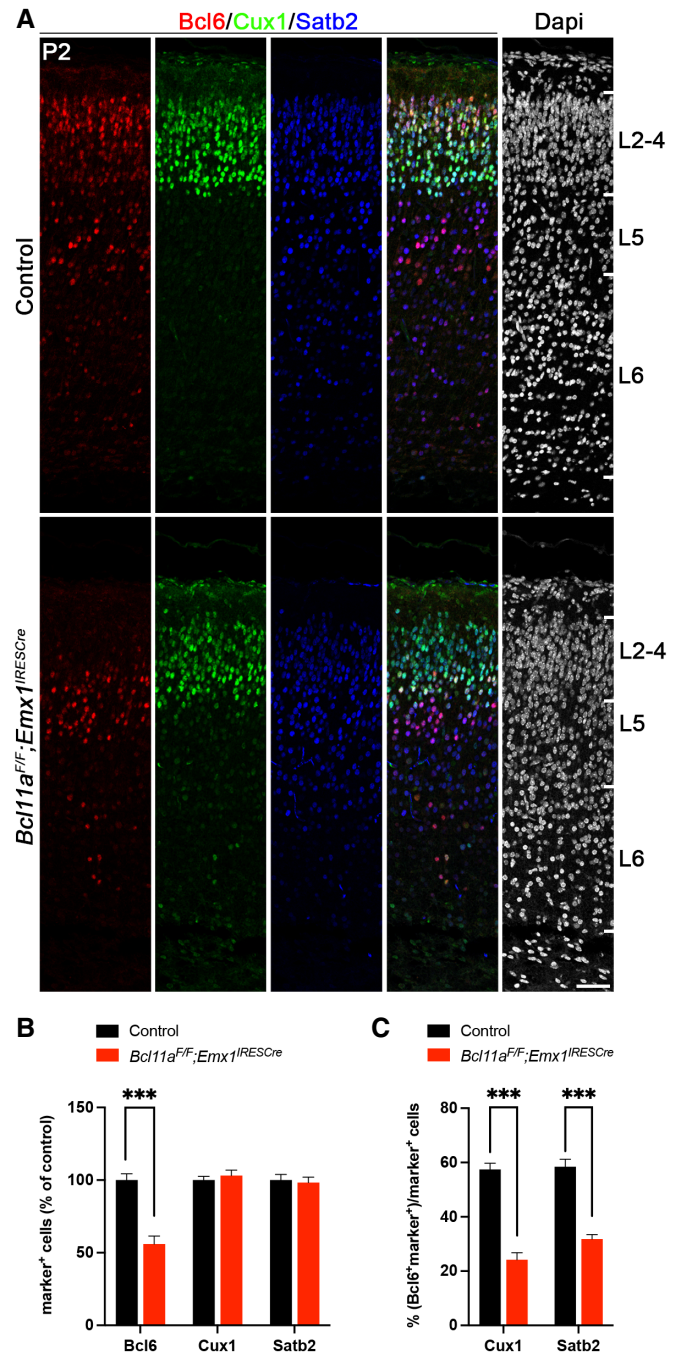## Bcl6 is downregulated in upper layers of *Bcl11a* mutant neocortex

To confirm Bcl6 downregulation in the *Bcl11a* mutant neocortex on protein level, we performed immunohistochemistry with Bcl6 and neuron subtype-specific antibodies. The overall expression of Bcl6 was reduced by $44.0 \pm 7.0\%$ compared with control neocortex at P2 (Fig 3A and B). We did not detect changes in the number of $Satb2^+$ and $Cux1^+$ cells that would normally coexpress with Bcl6 (c.f. Fig 2A–D), suggesting that these cells are born correctly, have for the most part migrated to their respective layers, and undergo neuron subtype-specific differentiation (Fig 3A and B). Furthermore, the proportion of $Cux1^+$ and $Satb2^+$ cells coexpressing Bcl6 was reduced from 57.4 ± 2.3 to $24.2 \pm 2.6\%$ and 58.5 ± 2.8 to $31.8 \pm 1.6\%$, respectively, in *Bcl11a* mutant compared with control neocortex (Fig 3A and C). As previously demonstrated, cortical thickness is reduced and layer 5 is increased at the expense of layer 6 in *Bcl11a* mutants at this stage (Wiegreffe *et al*, 2015; Woodworth *et al*, 2016). We did not detect significant changes in the number of cells coexpressing Bcl6 in deep cortical layers labeled by Bcl11b (layer 5) or Tbr1 (layer 6; Molyneaux *et al*, 2007; Fig EV4A–C), indicating a selective loss of Bcl6 in upper-layer neurons. Together, these data are compatible with a function of Bcl6 in CPN survival, which is massively impaired in upper layers of the *Bcl11a* mutant neocortex after P2 (Wiegreffe *et al*, 2015).

Cell-autonomous control of Bcl6 expression by *Bcl11a*

To further examine whether Bcl6 expression is directly regulated by Bcl11a in neurons, we created a mosaic mutant *in vivo* situation by using *in utero* electroporation. We generated *Bcl11a*-deficient neurons in cortical layer 2/3 by electroporating Cre together with GFP (CAG-Cre^{GFP}) or GFP alone (CAG-Ctl^{GFP}) into conditional *Bcl11a* mutant ($Bcl11a^{F/F}$) brains at E15.5 and analyzed the transfected brains at P2 (Fig 4A and B). The proportion of GFP^+ cells that coexpresses Bcl6 was reduced from $70.3 \pm 4.0\%$ in controls to $9.5 \pm 1.5\%$ in *Bcl11a*-deficient cortical neurons (Fig 4C and F). In contrast, the proportions of GFP^+ cells that coexpress Cux1 or Satb2 remained unchanged (Fig 4D–F). Thus, cell-autonomous loss of *Bcl11a* in superficial cortical layers leads to a dramatic and specific reduction of Bcl6. Together with the direct binding of Bcl11a to the Bcl6 gene and its transcriptional activation through a conserved binding motif (Fig 2E–G), this suggests that Bcl11a directly controls *Bcl6* expression in these cells.

Reintroduction of *Bcl6* into *Bcl11a* mutants rescues neuron death

We next asked whether reintroduction of *Bcl6* into *Bcl11a* mutant neurons located in upper cortical layers could rescue mutant neurons from undergoing apoptosis and thereby normalize the *Bcl11a* mutant phenotype. We generated Cre-dependent control (CAG-LSL-Ctl^{GFP}) and *Bcl6* (CAG-LSL-$Bcl6^{GFP}$) expression constructs that were tested in HEK293 cells and by western blot (Appendix Fig S2A). Both constructs induced robust *GFP* expression

Figure 3. Bcl6 expression is specifically downregulated in superficial cortical layers of $Bcl11a^{F/F};Emx1^{IRESCre}$ neocortex.

A Immunohistochemistry of Bcl6 (red), Cux1 (green), and Satb2 (blue) in P2 $Bcl11a^{F/F};Emx1^{IRESCre}$ and control neocortex. Nuclei are stained with Dapi (white).

B Relative quantification of $Bcl6^+$, $Satb2^+$, and $Cux1^+$ cells in $Bcl11a^{F/F};Emx1^{IRESCre}$ and control neocortex ($n = 4$).

C Numbers of $Cux1^+$ or $Satb2^+$ cells that coexpress Bcl6 are reduced in $Bcl11a^{F/F};Emx1^{IRESCre}$ compared with control neocortex ($n = 4$).

Data information: All graphs represent the mean $\pm$ s.e.m.; Student's t-test; ***$P < 0.001$. Scale bar, 50 μm.

in the presence or absence of *Cre*, indicating that the floxed stop (*LSL*) cassette did not prevent the *GFP* from being expressed. However, *Bcl6* expression was only observed in the presence of *Cre*, indicating a tight regulation of *Bcl6* expression from this construct (Appendix Fig S2B). We then overexpressed *Bcl6* in *Bcl11a* mutant cortical neurons by *in utero* electroporation at E15.5 and analyzed
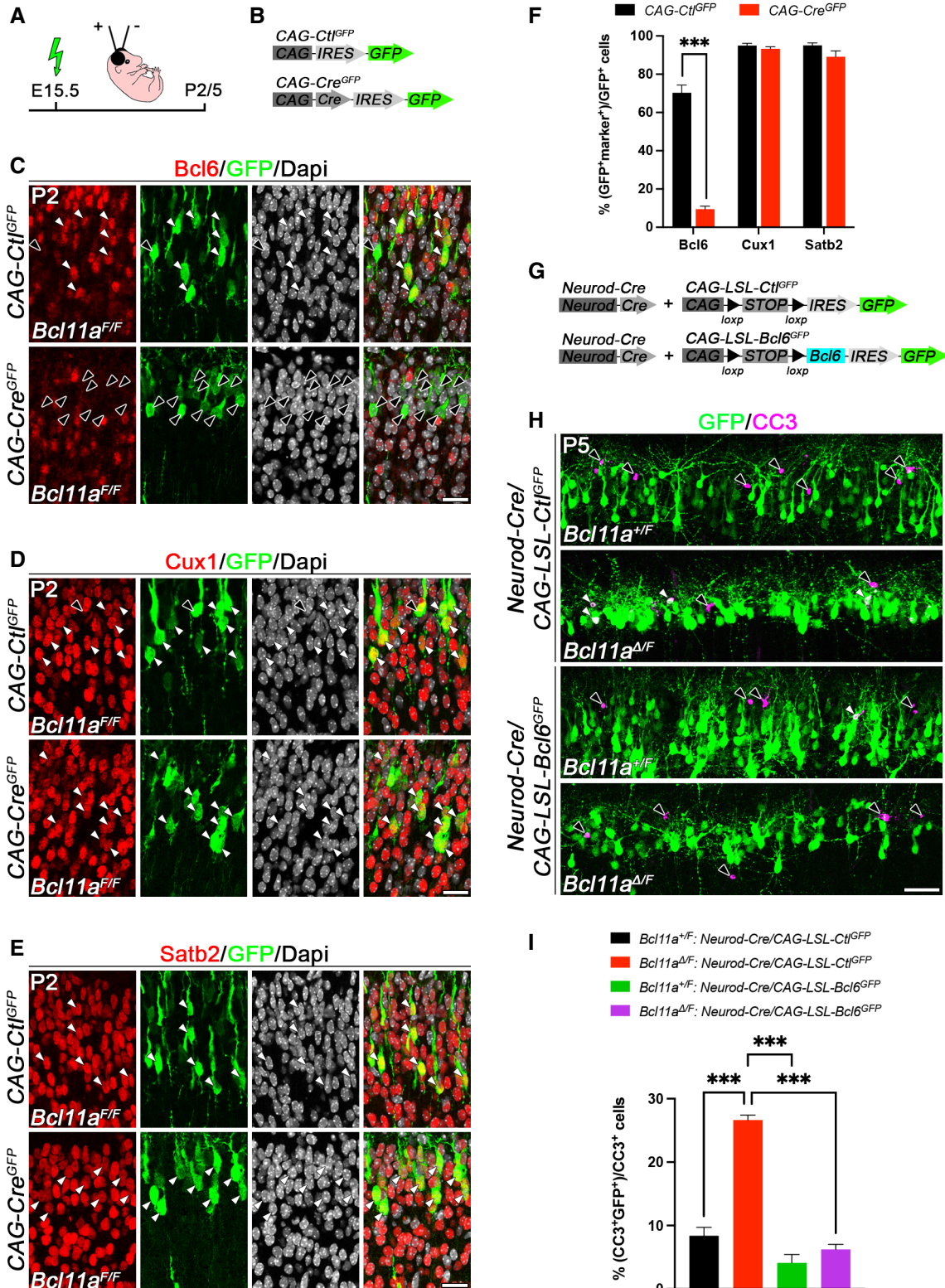

Figure 4.

◀

Figure 4. Cell-autonomous loss of *Bcl11a* in superficial cortical layers leads to reduced Bcl6 expression and reintroduction of *Bcl6* into *Bcl11a* mutant superficial projection neurons rescues the *Bcl11a* mutant phenotype.

A   Schematic representation of the experimental approach. Embryos are electroporated at E15.5 with the indicated DNA plasmids and sacrificed at either P2 or P5.
B   DNA plasmids used in the experiment shown in (C–F).
C–E   Immunohistochemistry of electroporated P2 *Bcl11a$^{F/F}$* neurons in superficial cortical layers with GFP (green) and Bcl6 (red, C), Cux1 (red, D), or Satb2 (red, E) antibodies. Bcl6 expression is specifically downregulated *Bcl11a$^{F/F}$* neocortex upon electroporation of *CAG-Cre^{GFP}* in comparison with *CAG-Ctl^{GFP}* control plasmid. Nuclei are stained with Dapi (white).
F   Quantification of the percentage of electroporated cells expressing Bcl6 (n = 3), Satb2 (n = 3), and Cux1 (n = 5). Results are expressed as mean ± s.e.m.; Student's *t*-test; ***P < 0.001.
G   DNA plasmids used in the experiment shown in (H and I).
H   Immunohistochemistry of electroporated P5 *Bcl11a$^{Δ/F}$* and *Bcl11a$^{+/F}$* neurons in superficial cortical layers with GFP (green) and cleaved caspase 3 (CC3, magenta) antibodies. Electroporation of *Neurod-Cre^{GFP}* plasmid together with *CAG-LSL-Bcl6^{GFP}* into *Bcl11a$^{F/F}$* neocortex reduces the number of CC3$^+$ cells to control levels.
I   Quantification of the experiment shown in (H) (n = 4). Results are expressed as mean ± s.e.m.; one-way ANOVA followed by Tukey's *post-hoc* test; ***P < 0.001.

Data information: White arrowheads point at GFP$^+$ cells that also express Bcl6, Cux1, Satb2, or CC3. Black arrowheads indicate cells expressing only GFP$^+$. Scale bars, 20 μm (C–E), 50 μm (H).

the brains at P5 (Fig 4A). To circumvent functions of *Bcl6* that could interfere with neurogenesis (Tiberi *et al*, 2012; Bonnefont *et al*, 2019), we directed *Bcl6* expression to postmitotic neurons by electroporating *CAG-LSL-Ctl^{GFP}* or *CAG-LSL-Bcl6^{GFP}* expression constructs together with *Cre* placed under the control of the postmitotically activated *Neurod* promoter (*Neurod-Cre*) into *Bcl11a$^{Δ/F}$* (i.e., conditional mutant) or *Bcl11a$^{+/F}$* (i.e., control) brains (Fig 4G). Co-electroporation of *Neurod-Cre* together with *CAG-LSL-Ctl^{GFP}* robustly induced cell death in *Bcl11a$^{Δ/F}$* in comparison with control brains by more than threefold. In contrast, postmitotic reintroduction of *Bcl6* into *Bcl11a*-deficient neurons reduced apoptosis to control levels. Of note, overexpression of *Bcl6* in control brains did not significantly reduce the number of cleaved caspase 3$^+$ cells below control levels (Fig 4H and I). Together, these data strongly support a role for *Bcl6* as a direct functional downstream target of Bcl11a that controls neuron survival during the second wave of DCD at the early postnatal stage.

Increased cell death in postnatal *Bcl6* mutant neocortex

To further corroborate that *Bcl6* confers survival of cortical projection neurons, we generated forebrain-specific *Bcl6* mutants by crossing conditional *Bcl6* mutant mice (*Bcl6$^{F/F}$*), in which exons 7–9 are

flanked by *loxP* sites (Hollister *et al*, 2013), with *Nex^{Cre}* mice (Goebbels *et al*, 2006) that induce recombination in postmitotic cortical projection neurons. Quantitative real-time PCR showed that *Nex^{Cre}* reduced *Bcl6* expression by 80.0 ± 0.1% compared with controls at P0 (Fig 5B). Due to restricted activity of *Nex^{Cre}*, incomplete reduction of Bcl6 is likely caused by residual expression in non-neuronal cell types. We chose P5 to analyze DCD in *Bcl6* mutant brains because *Bcl11a* mutants display massively increased cell death (Wiegreffe *et al*, 2015) and naturally occurring cell death in wild-type brains peaks around this stage (Blanquie *et al*, 2017). We found a significant increase in cleaved caspase 3$^+$ cells located predominantly in the upper cortical layers from 6.04 ± 0.02% in controls to 8.44 ± 0.77% cells/mm^2 in *Bcl6* mutant brains concomitant with a reduction of cortical area by 9.7 ± 2.0% (Fig 5A, C and D). We compared this increase in apoptosis in *Bcl6* mutants to the phenotypes observed in *Bcl11a$^{F/F}$;Nex^{Cre}* and the previously described *Bcl11a$^{F/F}$;Emx1^{IRESCre}* mutants (Fig EV5A and B; Wiegreffe *et al*, 2015). Both *Bcl11a* mutants display a similar extent of apoptosis. In both cases, increased neuron death was more pronounced as compared to the apoptosis rate observed in *Bcl6$^{F/F}$;Nex^{Cre}* mutants. This suggests that upstream of Bcl6, Bcl11a controls additional functions in neocortex development, which may indirectly and independently of Bcl6 contribute to cell survival control of CPN. For

Figure 5. Postnatal developmental cell death is increased in *Bcl6$^{F/F}$;Nex^{Cre}* neocortex.   ▶

A   Immunohistochemistry of cleaved caspase 3 (CC3) shows that the number of CC3$^+$ cells (marked by black arrowheads) is increased in P5 *Bcl6$^{F/F}$;Nex^{Cre}* compared with control neocortex. Insets are enlargements of the boxed areas in corresponding panels.
B   Relative *Bcl6* mRNA expression level determined by quantitative real-time PCR using primers targeting a region of exon 8 is decreased in P0 *Bcl6$^{F/F}$;Nex^{Cre}* compared with control brains (n = 4). Results are expressed as mean ± s.e.m.; Student's *t*-test; ***P < 0.001.
C   Quantification of the experiment shown in (A) (n = 3). Results are expressed as mean ± s.e.m.; Student's *t*-test; *P < 0.05.
D   Quantification of neocortical area in P5 *Bcl6$^{F/F}$;Nex^{Cre}* and control brains (n = 3). Results are expressed as mean ± s.e.m.; Student's *t*-test; **P < 0.01.
E   Heat map showing differentially expressed genes in laser-microdissected superficial cortical layers of P5 *Bcl6$^{F/F}$;Nex^{Cre}* compared with control brains (n = 4).
F   Relative *Foxo1* mRNA expression level determined by quantitative real-time PCR is increased in laser-microdissected superficial cortical layers of P5 *Bcl6$^{F/F}$;Nex^{Cre}* compared with control brains (n = 4). Results are expressed as mean ± s.e.m.; Student's *t*-test; **P < 0.01.
G   RNA *in situ* hybridization showing upregulation of *Foxo1* expression in P5 *Bcl6$^{F/F}$;Nex^{Cre}* compared with control neocortex.
H   Schematic representation of the experimental approach. Embryos are electroporated at E15.5 and sacrificed at P5.
I   DNA plasmids used in the experiment shown in (J and K).
J   Immunohistochemistry of electroporated P5 *Bcl11a$^{F/F}$* neurons in superficial cortical layers with GFP (green) and cleaved caspase 3 (CC3, magenta) antibodies. Electroporation of *CAG-Cre^{GFP}* plasmid together with *Foxo1-shRNA^{GFP}*#4 into *Bcl11a$^{F/F}$* neocortex reduces the number of CC3$^+$ cells to control levels. White and black arrowheads indicate GFP$^+$ CC3$^+$ and GFP$^+$ cells, respectively.
K   Quantification of the experiment shown in (J) (n = 4, *CAG-Ctl^{GFP}/Ctl-shRNA^{GFP}*; n = 3, *CAG-Cre^{GFP}/Ctl-shRNA^{GFP}*; n = 5, *CAG-Cre^{GFP}/Foxo1-shRNA^{GFP}*#4). Results are expressed as mean ± s.e.m.; one-way ANOVA followed by Tukey's *post-hoc* test; *P < 0.05.

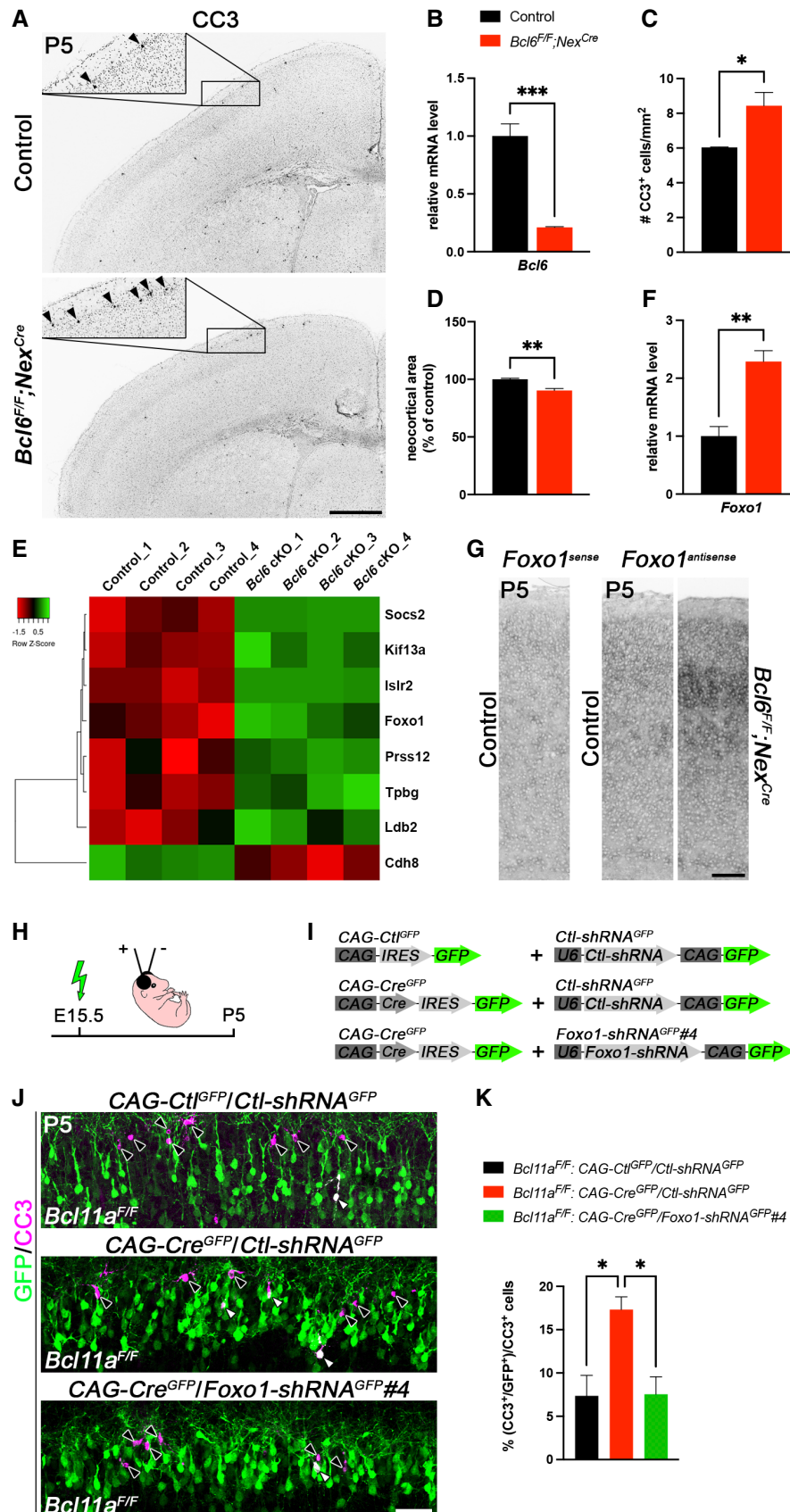Data information: Scale bars, 500 μm (A), 50 μm (G, J).

Figure 5.

example, we and others have shown previously that morphogenesis and connectivity of CPN depend on Bcl11a (Simon *et al*, 2020).

Collectively, our data show that Bcl6 exerts functions in upper-layer neuron survival during early postnatal neocortical development. To characterize downstream genetic pathways of Bcl6 responsible for the observed phenotype, we isolated upper cortical layers from *Bcl6* mutant and control brains by laser capture microdissection at P5 and performed a differential expression analysis on this tissue using microarrays. This analysis revealed a small number of DE genes that were mostly upregulated in *Bcl6* mutant upper cortical layers (Fig 5E, Dataset EV2). By systematic comparison of the differential transcriptomes of *Bcl11a* and *Bcl6* mutants (Datasets EV1 and EV2, and Fig EV5C), we identified only three genes overlapping in both datasets that were verified by quantitative real-time PCR (Fig EV5C–E). Of these genes, the cell death-associated factor Foxo1 was found upregulated in both, *Bcl6* and *Bcl11a* mutants (Fig 5F; Fig EV5D and E). Upregulation of *Foxo1* was most apparent in upper layers of the *Bcl6* mutant neocortex (Fig 5G). Bcl11a and Bcl6 were shown to physically interact and colocalize in nuclear paraspeckles suggesting common regulation of gene expression (Nakamura *et al*, 2000; Liu *et al*, 2006). Members of the Foxo family have been demonstrated to be involved in the control of neuron survival (Carter & Brunet, 2007; Santo & Paik, 2018). It might thus well be that Bcl6 together with Bcl11a exerts anti-apoptotic functions in CPN through this pathway.

To further explore functions of Foxo1 in Bcl11a/Bcl6-dependent DCD of CPN, we knocked down *Foxo1* gene expression by the help of shRNA according to previously published experimental strategies (Wiegreffe *et al*, 2015). The shRNA sequences were selected according to published studies (Zhang *et al*, 2011; Park *et al*, 2019). Using western blot analysis, construct *Foxo1-shRNA^{GFP}#4* was determined to be most efficient for its ability to reduce *Foxo1* expression and employed for further experiments (Appendix Fig S3A–C). Using *in utero* electroporation, we introduced *Foxo1-shRNA^{GFP}#4 together with CAG-Cre^{GFP}* constructs into *Bcl11a^{F/F}* upper-layer CPN. As controls, *Ctl-shRNA^{GFP}* together with *CAG-Ctl^{GFP}* or *CAG-Cre^{GFP}* were used. The shRNA-mediated knockdown of *Foxo1* expression was sufficient to suppress, that is, rescue the Bcl11a-dependent apoptosis phenotype in CPN *in vivo*. In contrast, co-electroporation of *Ctl-shRNA^{GFP}* together with *CAG-Cre^{GFP}* did not affect increased apoptosis in *Bcl11a* mutant CPN (Fig 5H–K). This provides direct experimental evidence for a functional role of Foxo1 in Bcl11a/Bcl6-dependent regulation of DCD of CPN. In lymphoid cells, Bcl6 regulates cell death through p53 function (Phan & Dalla-Favera, 2004; Cerchietti *et al*, 2008). Using quantitative real-time PCR, we did not detect changes in *p53* expression in our expression analysis (Fig EV5D and E). Taken together, in this study we demonstrate that DCD of postmitotic upper-layer CPN is controlled by a novel Bcl11a/Bcl6-dependent transcriptional pathway that involves Foxo1 function.

Previously, we demonstrated Bcl6 to be required during early phases of neocortical development, where Bcl6 promotes the transition of neural progenitors into postmitotic neurons (Tiberi *et al*, 2012; Bonnefont *et al*, 2019). Our data suggest additional functions of Bcl6 in the postnatal development of postmitotic CPN. A conserved function of this factor in control of cell survival is supported by its well-characterized functions in the lymphatic system. Bcl6 prevents apoptosis in germinal center B-cells and exerts oncogenic activity in diffuse large B-cell lymphoma both,

through modulation of the p53 downstream pathway (Phan & Dalla-Favera, 2004; Cerchietti *et al*, 2008). In the cerebellum, deletion of *Bcl6* induces massively increased cell death of granule cell precursors but not postmitotic granule cells leading to reduction of organ size (Tiberi *et al*, 2014). Interestingly, activation of nuclear calcium pathway through synaptic NMDA-receptor signaling induces Bcl6 expression in hippocampal neurons. In turn, upregulation of Bcl6 improves the survival of these neurons (Zhang *et al*, 2007). This suggests that activity-dependent as well as activity-independent, transcriptional regulatory pathways converge onto Bcl6 in the control of DCD.

Compared with *Bcl11a* mutants, we observed a milder increase in apoptosis in *Bcl6* mutant CPN, raising the possibility of additional signals to contribute to apoptosis in *Bcl11a* mutants, for example, through regulation of alternative cell death pathways. Our systematic GO and transcriptome analyses, however, did not reveal further candidate target genes of Bcl11a commonly involved in alternative apoptosis pathways. Postnatally, *Bcl11a* mutant CPN display severe morphogenetic defects as characterized by shortened apical dendrites and disturbed dendritic branching pattern (Wiegreffe *et al*, 2015). This may result in impaired synaptic integration and electrical activity of *Bc11a* mutant neurons and in turn contribute to the severity of the phenotype.

Alternatively, additional, not yet characterized signals, might be involved. In our screen, we detected several axon guidance molecules, including Slit2, Efna5, Sema3c, −3d, −7a, Flrt2, −3 to be deregulated in *Bcl11a* mutant CPN. Semaphorins, for example, have extensively been demonstrated to influence neuronal connectivity (Koropouli & Kolodkin, 2014). Thus, differentially expressed guidance molecules, as observed in our study, might either directly or indirectly, through modulation of connectivity influence the severity of the apoptosis phenotype in *Bcl11a* mutants. In addition, we found cadherin 6, 12, 13 and protocadherin 9 to be deregulated in *Bcl11a* mutant CPN. Recent experimental evidence suggests cadherins, in addition to their well-characterized functions in cell recognition and neural circuit assembly (Jontes, 2018; Sanes & Zipursky, 2020), to exert survival functions as well, for example, in neocortical interneurons (László *et al*, 2020). We previously demonstrated Bcl11a to be expressed in neocortical interneurons (Wiegreffe *et al*, 2015) raising the possibility that Bcl11a controls DCD also in these cells. During neocorticogenesis, DCD occurs in cell-type-specific and temporally distinct patterns. In mice, numbers of CPN are refined by DCD specifically between P4 and P6, whereas the time course of DCD in cortical interneurons is shifted to later developmental stages (Southwell *et al*, 2012; Blanquie *et al*, 2017; Wong *et al*, 2018). *Emx1^{IRESCre}-/Nex^{Cre}*-dependent recombination as used in our study restricts *Bcl11a* mutation selectively to CPN. Thus, a role of Bcl11a in cortical interneuron survival remains to be determined by cell-type-specific mutation of *Bcl11a* in interneurons.

Bcl11a has been previously demonstrated to directly interact with Nr2f1 (COUP-TFI). Moreover, in a very recent study Bcl1a was suggested to directly bind to the *Nr2f1* gene locus and suppress its transcription (Du *et al*, 2021) raising the question whether Nr2f1 is involved in Bcl11a-dependent control of late DCD in cortical projection neurons. Several lines of evidence argue against this assumption. (i) extensive phenotype analyses of *Nr2f1* mutants from various laboratories have implicated this factor in control of cortical progenitor proliferation as well as cortical patterning, and laminar

fate determination in postmitotic neurons (Tocco et al, 2021). Yet, a direct role for Nr2f1 in control of postmitotic neuron survival has not been reported. (ii) in our study, we did not detect deregulated Nr2f1 expression in Bcl11a nor in Bcl6 mutants as compared to controls. Interestingly, Bcl11a and Nr2f1 have been shown to be involved in establishing somatomotor *versus* somatosensory cortical area identity leading to a partial motorization of the mutant neocortex (Armentano et al, 2007; Greig et al, 2016). Interestingly, wild-type Bcl6 expression is lower in the somatomotor cortex as in the somatosensory cortex. Correspondingly, numbers of neurons eliminated by DCD are substantially higher in the somatomotor as compared to the somatosensory cortex (Blanquie et al, 2017). Nr2f1 might thus indirectly participate in the control of Bcl6 expression through the control of cortical area identity. Whether this occurs through direct protein interaction with Bcl11a or indirectly through mechanisms independent of Bcl11a remains to be determined.

Materials and Methods

Animals

Mice carrying a conditional knockout allele of Bcl11a (Bcl11a^F) have previously been described (John et al, 2012). These mice were crossed to Emx1^{IRESCre} (Gorski et al, 2002), Nex^{Cre} (Goebbels et al, 2006), or Deleter^{Cre} (Schwenk et al, 1995) mice to generate conditional Bcl11a$^{F/F}$;Emx1^{IRESCre}, conditional Bcl11a$^{F/F}$;Nex^{Cre}, and Bcl11a$^{Δ/+}$ heterozygous mutants, respectively. Bcl11a$^{F/+}$;Emx1^{IRESCre} littermates were phenotypically indistinguishable from Bcl11a$^{+/+}$; Emx1^{IRESCre} animals (Appendix Fig S4A and B) and served as controls throughout the study. Mice carrying a conditional knockout allele of Bcl6 (Bcl6^F; Hollister et al, 2013) were crossed to Nex^{Cre} mice to generate conditional Bcl6$^{F/F}$;Nex^{Cre} mutants. Bcl6$^{F/F}$ littermates without a Nex^{Cre} allele served as controls. Bcl6$^{+/−}$ mice have previously been described (Ye et al, 1997). Genotyping of the mice was performed by PCR. Animals were kept in a 12:12-h light–dark cycle and at a constant temperature (22 ± 1°C) in IVC cages. All mouse experiments were carried out in compliance with German law and approved by the respective government offices in Tübingen, Germany.

Immunohistochemistry and RNA in situ hybridization

Brains were fixed in 4% PFA in 0.1 M phosphate buffer (pH 7.4), embedded in OCT compound (Polysciences), and frozen sections were prepared at 14 μm for immunohistochemistry or 18 μm for RNA in situ hybridization as previously described (John et al, 2012; Simon et al, 2012). Paraffin and vibratome sections were prepared at 7 and 50 μm, respectively. All clones for non-radioactive RNA in situ hybridization, except for Flrt2 and Flrt3, which were a gift by Rüdiger Klein (Max Planck Institute of Neurobiology, Martinsried, Germany), were generated by reverse transcription PCR and oligonucleotides are listed in Table EV1.

The following antibodies were used: guinea pig anti-Bcl11a at 1:1,000 dilution (John et al, 2012), mouse anti-Bcl11a at 1:1,000 dilution (Abcam Cat# ab19487, RRID:AB_444947), rabbit anti-Bcl11a at 1:1,000 dilution (John et al, 2012), rat anti-Bcl11b at 1:1,000 dilution (Abcam Cat# ab18465, RRID:AB_2064130), rabbit

anti-cleaved Caspase 3 at 1:300 dilution (Cell Signaling Technology Cat# 9661, RRID:AB_2341188), rabbit anti-Cux1 at 1:500 dilution (Santa Cruz Biotechnology Cat# sc-13,024, RRID:AB_2261231), chicken anti-GFP at 1:2,000 dilution (Abcam Cat# ab13970, RRID: AB_300798), mouse anti-Satb2 at 1:1,000 dilution (Abcam Cat# ab51502, RRID:AB_882455), and rabbit anti-Tbr1 at 1:500 dilution (Abcam Cat# ab31940, RRID:AB_2200219). To generate anti-Bcl6 antiserum, guinea pigs were injected with a protein comprising amino acids 4–484 of mouse Bcl6 (NP_033874) and pooled sera were purified by affinity chromatography and used at 1:1,000 dilution. Biotin-conjugated, HRP-conjugated, and fluorescent secondary antibodies were purchased from Jackson ImmunoResearch and used at 1:500 dilution. Sections were counterstained with Dapi (Molecular Probes). Immunohistochemical detection of Bcl6 was performed on paraffin sections with antigen retrieval by boiling the section for 30 min in Tris-EDTA buffer, pH 9.0 and enhanced using tyramide signal amplification (Invitrogen) according to the manufacturer's instructions or an avidin/biotin-based peroxidase system and DAB substrate (Vector Laboratories). Cleaved caspase 3 was detected on frozen sections of conditional Bcl6 mutants using an avidin/biotin-based peroxidase system and DAB substrate (Vector Laboratories). All fluorescent images were examined on a TCS SP5II confocal microscope (Leica) and processed with Adobe Photoshop (RRID: SCR_014199) software.

Laser microdissection

All procedures were performed in an RNase-free environment. Cortical layers 2–4 were isolated from unfixed frozen sections via laser microdissection. Briefly, brains were quickly removed from the skull, washed in ice-cold PBS, frozen in OCT compound (Polysciences), and stored at −80°C. Sections were prepared at 20 μm and mounted on membrane-covered 1 mm PEN slides (Zeiss) that were UV-treated and coated with poly-L-lysine. Sections were fixed in ice-cold 70% EtOH for 1 min, incubated in 1% cresyl violet acetate solution (Waldeck) for 45 s, and washed in 70% EtOH and 100% EtOH for 1 min each. After a brief drying step on a 37°C warming plate, sections were immediately processed for laser microdissection using a PALM MicroBeam Rel.4.2 (Zeiss). Laser-microdissected tissue was lysed in RLT lysis buffer (Qiagen) containing 2-mercaptoethanol for 30 min on ice and stored at −80°C before total RNA extraction.

Plasmids

CAG-Ctl^{GFP} and CAG-Cre^{GFP} have previously been described (Hand et al, 2005; Wiegreffe et al, 2015). Bcl11a (NM_001242934) and Bcl11b (NM_001079883) were cloned by PCR using cDNA as template and inserted into CAG-Ctl^{GFP} to generate CAG-Bcl11a^{GFP} and CAG-Bcl11b^{GFP}, respectively. The recombinase Cre was from CAG-Cre^{GFP} and inserted into pNeuroD-ires-GFP (gift of Franck Polleux; RRID:Addgene_61403) to generate NeuroD-Cre. The ires-GFP cassette was cut from CAG-Ctl^{GFP} and inserted into pCALNL-GFP (gift of Connie Cepko; RRID:Addgene_13770) to generate CAG-LSL-Ctl^{GFP}. Bcl6 (NM_009744) was cloned by PCR using a cDNA clone (OriGene Tec. Cat.# MC203091) as template and inserted into CAG-LSL-Ctl^{GFP} to generate CAG-LSL-Bcl6^{GFP}. CAG-Cre was a gift of Connie Cepko (RRID:Addgene_13775). Foxo1 (NM_019739) was

cloned by PCR using a cDNA clone (OriGene Tec. Cat.# MC203091) as template and inserted into *pCAG-DsRed2-FLAG* (gift of Franck Polleux) to generate *CAG-Foxo1*[FLAG]. *Foxo1-shRNA*[GFP]*#2* and *#4* were generated by cloning published shRNAs directed against *Foxo1* (Zhang *et al*, 2011; Park *et al*, 2019) into the short hairpin vector, *pCA-b-EGFPm5-silencer-3* (gift of Matthieu Vermeren) using the oligonucleotide sequences listed in Table EV2. *Ctl-shRNA*[GFP] was generated by cloning a scrambled sequence (5′-TACGCGCATAAGATTAGGG-3′) with no significant homology to any known gene sequence from mouse or human (Kawauchi *et al*, 2006) into *pCA-b-EGFPm5-silencer-3*.

In utero electroporation

In utero electroporation was performed as previously described (Saito & Nakatsuji, 2001; Wiegreffe *et al*, 2017) with minor modifications. Briefly, pregnant dams were anesthetized with Isoflurane (Abbott) and 1–2 μl of plasmid DNA were injected per embryo at a concentration of 0.5–1.0 μg/μl per construct. Five millimeter electrodes (Nepagene) and five pulses of 40 V (50 ms ON, 950 ms OFF) generated by a CUY21 EDIT electroporator (Nepagene) were used to transfect cells in the dorsolateral ventricular zone.

Microarray analysis, GO enrichment analysis, and quantitative real-time PCR

Microarray analysis was performed as previously described (John *et al*, 2012; Simon *et al*, 2012) with minor modifications. Briefly, total RNA was isolated from laser-microdissected control and mutant samples ($n = 4$) using the RNeasy Micro Plus Kit (Qiagen). The isolated RNA was checked for purity and integrity using Nanodrop spectrophotometer and TapeStation (Agilent), respectively. Transcriptome analysis was performed using GeneChip Mouse Gene 1.0 ST Arrays (Affymetrix) and BRB-ArrayTools developed by Dr. Richard Simon and BRB-ArrayTools Development Team (http://linus.nci.nih.gov/BRB-ArrayTools.html).

DE genes identified by microarray analysis were subjected to a gene ontology (GO) enrichment analysis using PANTHER version 15.0 (released 2020-02-14) and overrepresentation test (released 2020-02-28) with default settings and mouse whole-genome as reference list (Mi *et al*, 2013).

Total RNA was reverse transcribed using the SensiFast cDNA Synthesis Kit (Bioline), and quantitative real-time PCR was performed using the LightCycler DNA Master SYBR Green I Kit in a LightCycler 480 System (Roche). Oligonucleotides used for quantitative real-time PCR are listed in Table EV1. The relative copy number of *Gapdh* RNA was quantified and used for normalization. Data were analyzed using the comparative C_T method (Schmittgen & Livak, 2008).

Chromatin immunoprecipitation and luciferase assay

Chromatin immunoprecipitation (ChIP) was carried out as previously described (Nelson *et al*, 2006) with minor modifications. Briefly, P0 cortical tissue was collected from wild-type pups, flash-frozen in liquid nitrogen, and stored at −80°C until ChIP. Tissue was disrupted in low sucrose buffer (320 mM sucrose, 10 mM HEPES, pH 8.0, 5 mM $CaCl_2$, 3 mM $Mg[CH_3COO]_2$, 1 mM DTT, 0.1 mM

EDTA, 0.1% Triton X-100) and fixed for 15 min at RT in 1% formaldehyde. After quenching with glycine solution, nuclei were washed in Nelson buffer (140 mM NaCl, 20 mM EDTA, pH 8.0, 50 mM Tris, pH 8.0, 1% Triton X-100, 0.5% NP-40) and disrupted in RIPA buffer (140 mM NaCl, 10 mM Tris, pH 8.0, 1 mM EDTA, pH 8.0, 1% SDS, 1% Triton X-100, 0.1% NaDOC). Chromatin was sonicated for 40 cycles (30 s ON/OFF) using a Bioruptor Plus (Diagenode) with high power settings. For each ChIP reaction, 15 μg of sheared chromatin was diluted 10 times with IP buffer (50 mM Tris, pH 8.0, 150 mM NaCl, 1% NP-40, 0.5% NaDOC, 20 mM EDTA, pH 8.0, 0.1% SDS) and incubated overnight at 4°C with 3 μl specific mouse monoclonal antibody recognizing Bcl11a (Abcam Cat# ab19487, RRID:AB_444947) or unspecific IgG1 antibody (Cell Signaling Technology Cat# 5415, RRID:AB_10829607), which served as a negative control. Twenty microliter of protein G magnetic beads (Invitrogen) were added to each ChIP reaction for 2 h at 4°C. After washing with IP buffer containing 0.1% SDS, LiCl buffer (500 mM LiCl, 100 mM Tris, pH 8.0, 1% NP-40, 1% NaDOC, 20 mM EDTA, pH 8.0), and TE buffer (10 mM Tris, pH 8.0, 1 mM EDTA, pH 8.0), DNA was eluted from beads and purified by phenol-chloroform extraction. The precipitated DNA was analyzed by quantitative real-time PCR using oligonucleotides recognizing a region containing a conserved Bcl11a binding motif (TGACCA) in the first intron of *Bcl6*. As negative controls, oligonucleotides were used recognizing a region of exon 5 of *Bcl6* and the *Hprt* promoter region, respectively. All oligonucleotide sequences are listed in Table EV1. ChIP quantitative real-time PCR data were analyzed by the comparative C_T method determining the fold enrichment of the immunoprecipitated DNA by the specific antibody versus IgG1 using the input as a reference.

The 93-bp region containing the conserved Bcl11a binding motif in the first intron of *Bcl6* was cloned into a *Gaussia* luciferase (GLuc) reporter vector containing a minimal CMV promoter (pEZX-GN03; Genecopoeia). This construct was transfected into HEK293 cells (ATCC Cat# PTA-4488, RRID:CVCL_0045) with *CAG-Ctl*[GFP] or *CAG-Bcl11a*[GFP] using Lipofectamine 2000 according to the manufacturer's instructions (Invitrogen). A reporter vector containing a 112-bp region of exon 5 of *Bcl6* and *CAG-Bcl11b*[GFP] was transfected as a control. pCMV-SEAP (secreted alkaline phosphatase) was co-transfected in each well as a transfection control. Supernatant from transfected cells was analyzed 48 h after transfection. Luciferase assays were performed using the Secrete-Pair Dual Luminescence Assay Kit (Genecopoeia) in accordance with the manufacturer's instructions and a SpectraMax i3x instrument (Molecular Devices). Values are reported as the mean ratio of luminescence intensity of GLuc over SEAP and were collected from four independent experiments performed with at least two replicates per experiment.

Cell culture and western blot

HEK293 cells (ATCC Cat# PTA-4488, RRID:CVCL_0045) were grown in DMEM with 10% fetal calf serum and 1% penicillin/streptomycin at 37°C under 5% CO_2 atmosphere. Cells were transfected using Lipofectamine 2000 according to the manufacturer's instructions (Invitrogen). After 48 h, total proteins were extracted with ice-cold lysis buffer (1% NP-40, 150 mM NaCl, 50 mM Tris, pH 8.0, 1 mM EDTA), separated by SDS–PAGE, and electrophoretically transferred onto PVDF membranes (Amersham). Membranes were blocked with 5% non-fat milk (Bio-Rad) and incubated with mouse anti-β-actin

(Abcam Cat# ab8226, RRID:AB_306371), rabbit anti-Bcl6 (Santa Cruz Biotechnology Cat# sc-858, RRID:AB_2063450), rabbit anti-FLAG (Sigma-Aldrich Cat# F7425, RRID:AB_439687), rabbit anti-Gapdh (Sigma-Aldrich Cat# G9545, RRID:AB_796208), and chicken anti-GFP (Abcam Cat# ab13970, RRID:AB_300798), followed by treatment with horseradish peroxidase-conjugated secondary antibodies (Jackson ImmunoResearch) and ECL Plus western blotting detection reagents (ThermoScientific) or DAB substrate (Vector Laboratories) according to the manufacturers' instructions.

Cell counts and statistical analysis

For each experiment, at least three control and three mutant brains were analyzed, and three to five sections per brain were quantified. Anatomically matched sections were selected from an anterio-posterior level between the anterior commissure and the dorsal hippocampus. Stained cells were counted in radial units of 100 μm (Figs 2, 3 and EV4), 350 μm (Fig 4C–F), or 750 μm (Figs 4H and I, and 5J and K) width in the presumptive somatosensory cortex or in the entire neocortex (Figs 5A and C, and EV5A and B, Appendix Fig S4). Cells were counted using ImageJ (RRID:SCR_003070) and Imaris (RRID:SCR:007370) software. Statistical analysis was done with Microsoft Excel (RRID:SCR_016137) or GraphPad Prism (RRID:SCR_002798) software. Venn diagrams were generated using MATLAB (RRID:SCR_001622) software. Significance between groups was assessed using a two-tailed Student's *t*-test or one-way ANOVA, followed by Tuckey's *post-hoc* test. *P*-values < 0.05 were considered statistically significant.

Data availability

The datasets produced in this study are available in the following databases:

i microarray data: Gene Expression Omnibus GSE185287 (https://www.ncbi.nlm.nih.gov/geo/query/acc.cgi?acc=GSE185287).
ii microarray data: Gene Expression Omnibus GSE185288 (https://www.ncbi.nlm.nih.gov/geo/query/acc.cgi?acc=GSE185288).

Expanded View for this article is available online.

Author contributions

Christoph Wiegreffe: Conceptualization; validation; investigation; visualization; methodology. **Tobias Wahl:** Investigation. **Natalie Sophie Joos:** Investigation. **Jerome Bonnefont:** Resources. **Pentao Liu:** Resources. **Stefan Britsch:** Conceptualization; supervision.

Disclosure and competing interests statement

The authors declare that they have no conflict of interest.

References

Alcamo EA, Chirivella L, Dautzenberg M, Dobreva G, Farinas I, Grosschedl R, McConnell SK (2008) Satb2 regulates callosal projection neuron identity in the developing cerebral cortex. *Neuron* 57: 364–377

Armentano M, Chou SJ, Tomassy GS, Leingartner A, O'Leary DD, Studer M (2007) COUP-TFI regulates the balance of cortical patterning between frontal/motor and sensory areas. *Nat Neurosci* 10: 1277–1286

Avram D, Fields A, Senawong T, Topark-Ngarm A, Leid M (2002) COUP-TF (chicken ovalbumin upstream promoter transcription factor)-interacting protein 1 (CTIP1) is a sequence-specific DNA binding protein. *Biochem J* 368: 555–563

Blanquie O, Yang JW, Kilb W, Sharopov S, Sinning A, Luhmann HJ (2017) Electrical activity controls area-specific expression of neuronal apoptosis in the mouse developing cerebral cortex. *eLife* 6: e27696

Blaschke AJ, Staley K, Chun J (1996) Widespread programmed cell death in proliferative and postmitotic regions of the fetal cerebral cortex. *Development* 122: 1165–1174

Bonnefont J, Tiberi L, van den Ameele J, Potier D, Gaber ZB, Lin X, Bilheu A, Herpoel A, Velez Bravo FD, Guillemot F *et al* (2019) Cortical neurogenesis requires Bcl6-mediated transcriptional repression of multiple self-renewal-promoting extrinsic pathways. *Neuron* 103: e1094

Britanova O, de Juan RC, Cheung A, Kwan KY, Schwark M, Gyorgy A, Vogel T, Akopov S, Mitkovski M, Agoston D *et al* (2008) Satb2 is a postmitotic determinant for upper-layer neuron specification in the neocortex. *Neuron* 57: 378–392

Carter ME, Brunet A (2007) FOXO transcription factors. *Curr Biol* 17: R113–R114

Causeret F, Coppola E, Pierani A (2018) Cortical developmental death: selected to survive or fated to die. *Curr Opin Neurobiol* 53: 35–42

Cerchietti LC, Polo JM, Da Silva GF, Farinha P, Shaknovich R, Gascoyne RD, Dowdy SF, Melnick A (2008) Sequential transcription factor targeting for diffuse large B-cell lymphomas. *Cancer Res* 68: 3361–3369

Chowdhury TG, Jimenez JC, Bomar JM, Cruz-Martin A, Cantle JP, Portera-Cailliau C (2010) Fate of cajal-retzius neurons in the postnatal mouse neocortex. *Front Neuroanat* 4: 10

De Bruyckere E, Simon R, Nestel S, Heimrich B, Katzel D, Egorov AV, Liu P, Jenkins NA, Copeland NG, Schwegler H *et al* (2018) Stability and function of hippocampal mossy fiber synapses depend on Bcl11b/Ctip2. *Front Mol Neurosci* 11: 103

de la Rosa EJ, de Pablo F (2000) Cell death in early neural development: beyond the neurotrophic theory. *Trends Neurosci* 23: 454–458

Denaxa M, Neves G, Burrone J, Pachnis V (2018) Homeostatic regulation of interneuron apoptosis during cortical development. *J Exp Neurosci* 12: 1179069518784277

Du H, Wang Z, Guo R, Yang L, Liu G, Zhang Z, Xu Z, Tian Y, Yang Z, Li X *et al* (2021) Transcription factors Bcl11a and Bcl11b are required for the production and differentiation of cortical projection neurons. *Cereb Cortex* bhab437

Eriksson SH, Thom M, Heffernan J, Lin WR, Harding BN, Squier MV, Sisodiya SM (2001) Persistent reelin-expressing Cajal-Retzius cells in polymicrogyria. *Brain* 124: 1350–1361

Goebbels S, Bormuth I, Bode U, Hermanson O, Schwab MH, Nave KA (2006) Genetic targeting of principal neurons in neocortex and hippocampus of NEX-Cre mice. *Genesis* 44: 611–621

Gorski JA, Talley T, Qiu M, Puelles L, Rubenstein JL, Jones KR (2002) Cortical excitatory neurons and glia, but not GABAergic neurons, are produced in the Emx1-expressing lineage. *J Neurosci* 22: 6309–6314

Greig LC, Woodworth MB, Greppi C, Macklis JD (2016) Ctip1 controls acquisition of sensory area identity and establishment of sensory input fields in the developing neocortex. *Neuron* 90: 261–277

Hand R, Bortone D, Mattar P, Nguyen L, Heng JI, Guerrier S, Boutt E, Peters E, Barnes AP, Parras C *et al* (2005) Phosphorylation of Neurogenin2 specifies the migration properties and the dendritic morphology of pyramidal neurons in the neocortex. *Neuron* 48: 45–62

Hollister K, Kusam S, Wu H, Clegg N, Mondal A, Sawant DV, Dent AL (2013) Insights into the role of Bcl6 in follicular Th cells using a new conditional mutant mouse model. *J Immunol* 191: 3705–3711

Huang EJ, Reichardt LF (2001) Neurotrophins: roles in neuronal development and function. *Annu Rev Neurosci* 24: 677–736

John A, Brylka H, Wiegreffe C, Simon R, Liu P, Juttner R, Crenshaw EB 3rd, Luyten FP, Jenkins NA, Copeland NG *et al* (2012) Bcl11a is required for neuronal morphogenesis and sensory circuit formation in dorsal spinal cord development. *Development* 139: 1831–1841

Jontes JD (2018) The cadherin superfamily in neural circuit assembly. *Cold Spring Harb Perspect Biol* 10: a029306

Kawauchi T, Chihama K, Nabeshima Y, Hoshino M (2006) Cdk5 Phosphorylates and stabilizes p27kip1 contributing to Actin organization and cortical neuronal migration. *Nat Cell Biol* 8: 17–26

Koropouli E, Kolodkin AL (2014) Semaphorins and the dynamic regulation of synapse assembly, refinement, and function. *Curr Opin Neurobiol* 27: 1–7

Kuida K, Zheng TS, Na S, Kuan C, Yang D, Karasuyama H, Rakic P, Flavell RA (1996) Decreased apoptosis in the brain and premature lethality in CPP32-deficient mice. *Nature* 384: 368–372

László ZI, Bercsényi K, Mayer M, Lefkovics K, Szabó G, Katona I, Lele Z (2020) N-cadherin (Cdh2) maintains migration and postmitotic survival of cortical interneuron precursors in a cell-type-specific manner. *Cereb Cortex* 30: 1318–1329

Ledonne F, Orduz D, Mercier J, Vigier L, Grove EA, Tissir F, Angulo MC, Pierani A, Coppola E (2016) Targeted inactivation of Bax reveals a subtype-specific mechanism of Cajal-Retzius neuron death in the postnatal cerebral cortex. *Cell Rep* 17: 3133–3141

Liu H, Ippolito GC, Wall JK, Niu T, Probst L, Lee BS, Pulford K, Banham AH, Stockwin L, Shaffer AL *et al* (2006) Functional studies of BCL11A: characterization of the conserved BCL11A-XL splice variant and its interaction with BCL6 in nuclear paraspeckles of germinal center B cells. *Mol Cancer* 5: 18

Liu N, Hargreaves VV, Zhu Q, Kurland JV, Hong J, Kim W, Sher F, Macias-Trevino C, Rogers JM, Kurita R *et al* (2018) Direct promoter repression by BCL11A controls the fetal to adult hemoglobin switch. *Cell* 173: e417

Mi H, Muruganujan A, Casagrande JT, Thomas PD (2013) Large-scale gene function analysis with the PANTHER classification system. *Nat Protoc* 8: 1551–1566

Molyneaux BJ, Arlotta P, Menezes JR, Macklis JD (2007) Neuronal subtype specification in the cerebral cortex. *Nat Rev Neurosci* 8: 427–437

Nakamura A, Swahari V, Plestant C, Smith I, McCoy E, Smith S, Moy SS, Anton ES, Deshmukh M (2016) Bcl-xL is essential for the survival and function of differentiated neurons in the cortex that control complex behaviors. *J Neurosci* 36: 5448–5461

Nakamura T, Yamazaki Y, Saiki Y, Moriyama M, Largaespada DA, Jenkins NA, Copeland NG (2000) Evi9 encodes a novel zinc finger protein that physically interacts with BCL6, a known human B-cell proto-oncogene product. *Mol Cell Biol* 20: 3178–3186

Nelson JD, Denisenko O, Bomsztyk K (2006) Protocol for the fast chromatin immunoprecipitation (ChIP) method. *Nat Protoc* 1: 179–185

Nieto M, Monuki ES, Tang H, Imitola J, Haubst N, Khoury SJ, Cunningham J, Gotz M, Walsh CA (2004) Expression of Cux-1 and Cux-2 in the subventricular zone and upper layers II-IV of the cerebral cortex. *J Comp Neurol* 479: 168–180

Park MK, Yao Y, Xia W, Setijono SR, Kim JH, Vila IK, Chiu HH, Wu Y, Billalabeitia EG, Lee MG *et al* (2019) PTEN self-regulates through USP11 via the PI3K-FOXO pathway to stabilize tumor suppression. *Nat Commun* 10: 636

Phan RT, Dalla-Favera R (2004) The BCL6 proto-oncogene suppresses p53 expression in germinal-Centre B cells. *Nature* 432: 635–639

Phan RT, Saito M, Basso K, Niu H, Dalla-Favera R (2005) BCL6 interacts with the transcription factor Miz-1 to suppress the cyclin-dependent kinase inhibitor p21 and cell cycle arrest in germinal center B cells. *Nat Immunol* 6: 1054–1060

Priya R, Paredes MF, Karayannis T, Yusuf N, Liu X, Jaglin X, Graef I, Alvarez-Buylla A, Fishell G (2018) Activity regulates cell death within cortical interneurons through a calcineurin-dependent mechanism. *Cell Rep* 22: 1695–1709

Ranuncolo SM, Polo JM, Dierov J, Singer M, Kuo T, Greally J, Green R, Carroll M, Melnick A (2007) Bcl-6 mediates the germinal center B cell phenotype and lymphomagenesis through transcriptional repression of the DNA-damage sensor ATR. *Nat Immunol* 8: 705–714

Roth KA, Kuan C, Haydar TF, D'Sa-Eipper C, Shindler KS, Zheng TS, Kuida K, Flavell RA, Rakic P (2000) Epistatic and independent functions of caspase-3 and Bcl-X(L) in developmental programmed cell death. *Proc Natl Acad Sci USA* 97: 466–471

Saito T, Nakatsuji N (2001) Efficient gene transfer into the embryonic mouse brain using in vivo electroporation. *Dev Biol* 240: 237–246

Sanes JR, Zipursky SL (2020) Synaptic specificity, recognition molecules, and assembly of neural circuits. *Cell* 181: 536–556

Santo EE, Paik J (2018) FOXO in neural cells and diseases of the nervous system. *Curr Top Dev Biol* 127: 105–118

Schmittgen TD, Livak KJ (2008) Analyzing real-time PCR data by the comparative C(T) method. *Nat Protoc* 3: 1101–1108

Schwenk F, Baron U, Rajewsky K (1995) A cre-transgenic mouse strain for the ubiquitous deletion of loxP-flanked gene segments including deletion in germ cells. *Nucleic Acids Res* 23: 5080–5081

Simon R, Brylka H, Schwegler H, Venkataramanappa S, Andratschke J, Wiegreffe C, Liu P, Fuchs E, Jenkins NA, Copeland NG *et al* (2012) A dual function of Bcl11b/Ctip2 in hippocampal neurogenesis. *EMBO J* 31: 2922–2936

Simon R, Wiegreffe C, Britsch S (2020) Bcl11 transcription factors regulate cortical development and function. *Front Mol Neurosci* 13: 51

Southwell DG, Paredes MF, Galvao RP, Jones DL, Froemke RC, Sebe JY, Alfaro-Cervello C, Tang Y, Garcia-Verdugo JM, Rubenstein JL *et al* (2012) Intrinsically determined cell death of developing cortical interneurons. *Nature* 491: 109–113

Tiberi L, Bonnefont J, van den Ameele J, Le Bon SD, Herpoel A, Bilheu A, Baron BW, Vanderhaeghen P (2014) A BCL6/BCOR/SIRT1 complex triggers neurogenesis and suppresses medulloblastoma by repressing sonic hedgehog signaling. *Cancer Cell* 26: 797–812

Tiberi L, van den Ameele J, Dimidschstein J, Piccirilli J, Gall D, Herpoel A, Bilheu A, Bonnefont J, Iacovino M, Kyba M *et al* (2012) BCL6 controls neurogenesis through Sirt1-dependent epigenetic repression of selective notch targets. *Nat Neurosci* 15: 1627–1635

Tocco C, Bertacchi M, Studer M (2021) Structural and functional aspects of the neurodevelopmental gene NR2F1: From animal models to human pathology. *Front Mol Neurosci* 14: 767965

Verney C, Takahashi T, Bhide PG, Nowakowski RS, Caviness VS Jr (2000) Independent controls for neocortical neuron production and histogenetic cell death. *Dev Neurosci* 22: 125–138

Wei H, Alberts I, Li X (2014) The apoptotic perspective of autism. *Int J Dev Neurosci* 36: 13–18

Wiegreffe C, Feldmann S, Gaessler S, Britsch S (2017) Time-lapse confocal imaging of migrating neurons in organotypic slice culture of embryonic mouse brain using in utero electroporation. *J Vis Exp* 55886

Wiegreffe C, Simon R, Peschkes K, Kling C, Strehle M, Cheng J, Srivatsa S, Liu P, Jenkins NA, Copeland NG *et al* (2015) Bcl11a (Ctip1) controls migration of cortical projection neurons through regulation of Sema3c. *Neuron* 87: 311–325

Wong FK, Bercsenyi K, Sreenivasan V, Portales A, Fernandez-Otero M, Marin O (2018) Pyramidal cell regulation of interneuron survival sculpts cortical networks. *Nature* 557: 668–673

Wong FK, Marin O (2019) Developmental cell death in the cerebral cortex. *Annu Rev Cell Dev Biol* 35: 523–542

Woodworth MB, Greig LC, Liu KX, Ippolito GC, Tucker HO, Macklis JD (2016) Ctip1 regulates the balance between specification of distinct projection neuron subtypes in deep cortical layers. *Cell Rep* 15: 999–1012

Ye BH, Cattoretti G, Shen Q, Zhang J, Hawe N, de Waard R, Leung C, Nouri-Shirazi M, Orazi A, Chaganti RS *et al* (1997) The BCL-6 proto-oncogene controls germinal-Centre formation and Th2-type inflammation. *Nat Genet* 16: 161–170

Zhang SJ, Steijaert MN, Lau D, Schutz G, Delucinge-Vivier C, Descombes P, Bading H (2007) Decoding NMDA receptor signaling: Identification of genomic programs specifying neuronal survival and death. *Neuron* 53: 549–562

Zhang X, Yalcin S, Lee DF, Yeh TY, Lee SM, Su J, Mungamuri SK, Rimmele P, Kennedy M, Sellers R *et al* (2011) FOXO1 is an essential regulator of pluripotency in human embryonic stem cells. *Nat Cell Biol* 13: 1092–1099